

Article

Theoretical Studies of Photophysical Properties of D- π -A- π -D-Type Diketopyrrolopyrrole-Based Molecules for Organic Light-Emitting Diodes and Organic Solar Cells

Ruifa Jin *, Xiaofei Zhang and Wenmin Xiao

College of Chemistry and Life Science, Inner Mongolia Key Laboratory of Photoelectric Functional Materials, Chifeng University, Chifeng 024000, China; skyinthefifthday@126.com (X.Z.); xiaowenmin6868@163.com (W.X.)

* Correspondence: Ruifajin@163.com; Tel./Fax: +86-0476-8300370

Academic Editor: Jwo-Huei Jou

Received: 14 December 2019; Accepted: 3 February 2020; Published: 4 February 2020



Abstract: A series of D- π -A diketopyrrolopyrrole(DPP)-based small molecules were designed for organic light-emitting diode(OLEDs) and organic solar cell(OSCs) applications. Applying the PBE0/6-31G(d,p) method, the ground state geometry and relevant electronic properties were investigated. The first excited singlet state geometry and the absorption and fluorescent spectra were simulated at the TD-PBE0/6-31G(d,p) level. The calculated results revealed that the photophysical properties were affected through the introduction of different end groups. Furthermore, the electronic transitions corresponding to absorption and emission exhibited an intramolecular charge transfer feature. Our results suggest that the designed molecules acted not only as luminescent for OLEDs, but also as donor materials in OSCs. Moreover, they can also be used as potential electron transfer materials for OLEDs and OSCs.

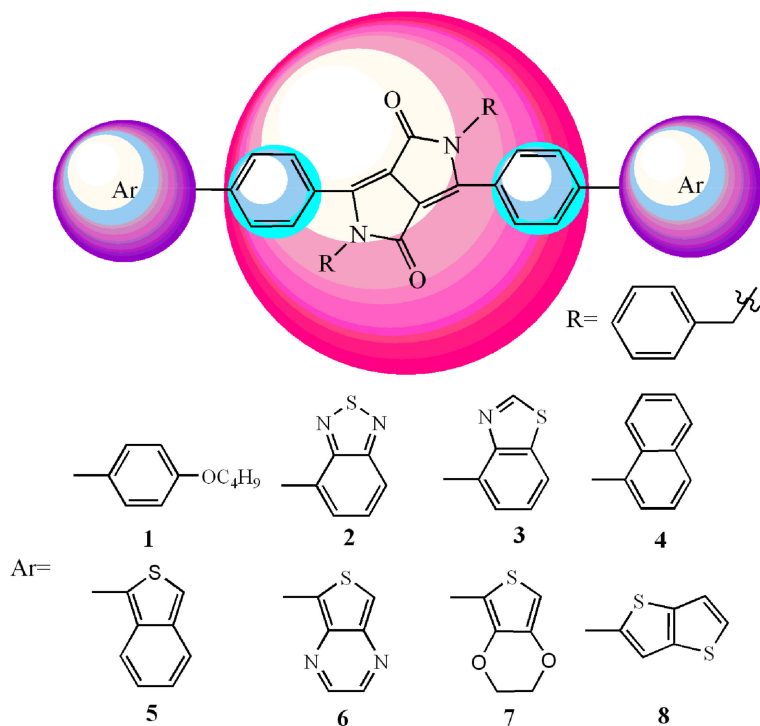
Keywords: diketopyrrolopyrrole(DPP)-based molecules; photophysical properties; Charge transporting property; organic light-emitting diodes(OLEDs); organic solar cells(OSCs)

1. Introduction

Organic semiconductors have attracted considerable interest in recent years due to their advantages over their inorganic counterparts, such as low-cost, lightweight, and flexible electronic devices [1–5]. In particular, small-molecule-based organic semiconductors are expected to open new possibilities in terms of optoelectronic applications in organic electronic devices including organic light-emitting diodes (OLEDs), organic solar cells (OSCs), and field effect transistors (FETs). Small-molecule-based organic semiconductors exhibit strong absorption and emission, high fluorescence quantum yields, and good charge carrier mobility [6]. Nevertheless, the lower efficiency of OLEDs and OSCs has seriously restricted their commercialization. The development of new small molecular materials with highly desirable properties remains a major challenge. Therefore, it is critically important to design and synthesize efficient multifunctional materials. These materials can serve as efficient light emitters in OLEDs, donor material for OSCs, and, simultaneously, charge transport materials [7,8]. In order to achieve high performance and enhance the power conversion efficiency (PCE) of OSCs, the frontier molecular orbitals (FMOs) energy levels of donors should match the typical acceptors. A deep HOMO (highest occupied molecular orbital) energy provides a high open circuit voltage (V_{oc}). A relatively high LUMO (lowest unoccupied molecular orbital) energy ensures efficient charge separation. [9,10] Additionally, a lower HOMO–LUMO gap (E_g) and strong absorption are required for effective harvesting of the solar photons. High charge-carrier mobility is also demanded for fast charge-carrier transport to maximize the short-circuit current (J_{sc}). Furthermore, another key

parameter is the downhill energetic driving force (ΔE_{L-L}), which is strongly related to the efficient charge transfer. The ΔE_{L-L} can be estimated by the energy difference between the LUMO of donor and acceptor, which should amount to at least 0.3 eV [11,12]. Normally, the fullerene derivatives PC₆₁BM ([6,6]-phenyl-C₆₁-butyric acid methyl ester), bisPC₆₁BM, and PC₇₁BM are employed as acceptors in OSCs [13,14]. Nowadays, one of the most efficient strategies for optoelectronic materials is to design and synthesize donor-acceptor molecular systems containing a π -bridged(D- π -A) framework [15–18]. The electronic energy levels, absorption and emission spectra, intermolecular stacking, and film morphology can be tuned effectively through chemical modification of the acceptor, donor, and π -bridge fragments [19–21]. Amongst various small molecular material building blocks, such as benzofuran [22], triphenylamine (TPA) units [23], tetraphenylethylene (TPE) [24], selenophene [25], phenanthrene [26], pyrene [27], and diketopyrrolopyrrole (DPP) derivative, DPP derivatives have attracted much interest owing to their outstanding performance in OSCs, OLEDs, and FETs [28–31]. DPP-containing materials possess promising features such as strong absorption and emission in the visible region, excellent thermal and photo-stability, large Stokes shift, and straightforward synthetic modification [32–36]. The DPP unit is a widely recognized electron acceptor owing to its strong electron-withdrawing nature [37,38]. In the D- π -A molecular systems containing DPP as core, the introduction of aromatic blocks at the 2,5 position of the DPP core can tune the optical properties via π - π intermolecular interactions. Furthermore, the introduction of various end-capping groups onto the aromatic blocks can further tune the molecular properties. Recently, it has been reported that some multifunctional DPP derivatives exhibit good optical properties [39].

In the present work, we designed several D- π -A- π -D-structured DPP-based small molecules for OSC and OLED applications. These molecules consist of the electron deficient DPP as the core (acceptor), different planar electron-rich aromatic groups as end groups (donor), and benzene as π -bridge (Scheme 1). Via the density functional theory (DFT) and time-dependent DFT (TD-DFT) computational approach, the photophysical and charge transfer properties were systematically investigated. The FMO energies (E_{HOMO} and E_{LUMO}), E_g , ΔE_{L-L} , reorganization energy (λ), and absorption and fluorescent spectra were predicted.



Scheme 1. Molecular structures of the investigated molecules.

2. Results and Discussion

2.1. Frontier Molecular Orbitals

To gain insight into the influence of the FMO energies on the optical and electronic properties, we examined the HOMO and LUMO contour plots of the designed molecules, as shown in Figure 1. On the basis of Mulliken population analysis, we also investigated the distribution patterns of FMOs using percentage contributions from DPP, π -bridge(BB), and end group(EG) moieties by means of partial density of states (PDOS) (see Table 1). The E_{HOMO} , E_{LUMO} , and E_g of 1–8 are plotted in Figure 2. Obviously, the FMOs exhibited π -orbital and strong delocalization features for 1–8, as shown in Figure 2. It was quite obvious that, comparing the contributions of DPP, BB, and EG fragments to the LUMOs with HOMOs, the DPP fragment contributions to LUMOs were smaller than those to HOMOs for 1–4 and 6–8, respectively. In contrast, the contribution of DPP fragment to LUMO was larger than that to HOMO for 5. For the contributions of BB fragments, the contributions to LUMOs were larger than those to HOMOs for 1–5, 7, and 8, respectively. The contribution to LUMO was smaller than that to HOMO for 6. For EG fragments, the contributions to LUMOs were larger than those to HOMOs for 2, 3, and 6 respectively. However, the contributions to LUMOs were smaller than those to HOMOs for 1, 4, 5, 7, and 8, respectively.

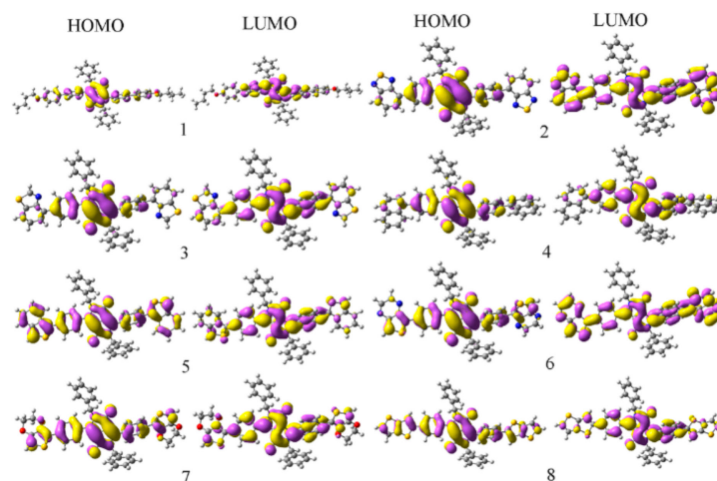


Figure 1. The electronic density contours of the frontier orbital for the studied compounds at the PBE0/6-31G (d,p) level.

Table 1. The highest occupied molecular orbital (HOMO) and lowest unoccupied molecular orbital (LUMO) contributions of individual fragments (in%) to the frontier molecular orbitals (FMOs) of 1–8 at the PBE0/6-31G (d,p) level.

Species	HOMOs			LUMOs		
	DPP ^a	CB ^b	Ar ^c	DPP	CB	Ar
1	71.0	19.2	9.8	66.1	28.5	5.4
2	75.3	19.0	5.7	33.9	21.1	45.0
3	75.5	19.4	5.1	60.2	30.3	9.5
4	73.1	19.0	7.9	64.3	30.2	5.6
5	47.3	19.7	33.0	54.8	29.8	15.5
6	63.9	21.3	14.9	28.3	21.1	50.6
7	61.2	22.6	16.3	58.2	30.4	11.5
8	61.3	21.0	17.7	56.3	31.1	12.5

^a DPP: diketopyrrolopyrrole fragment; ^b CB: conjugate bridge moieties; ^c Ar: aromatic groups.

Inspection of the results displayed in Table 1 revealed clearly that the excitation of the electron from the HOMOs to LUMOs led the electronic density to flow mainly from the **DPP** and **AR** fragments

to CB fragments for 1, 4, 7 and 8. For 2, 3, and 6, the electronic densities mainly flowed from DPP fragments to AR and CB fragments. However, the electronic density mainly flowed from the AR fragments to DPP and CB fragment for 5. This suggests that the different AR groups had obvious effects on the distribution of FMOs for the designed compounds. The percentages of charge transfer from DPP and AR fragments to CB fragments were 9.3%, 11.2%, 7.8%, and 10.1% for 1, 4, 7, and 8, respectively. For 2, 3, and 6, the percentages of charge transfer from DPP fragments to AR and CB fragments were 41.4%, 15.3%, and 35.6%, respectively. The percentage of charge transfer from AR to DPP and BB fragment for 5 was 35.6%. Therefore, the order of the electron-donor ability of end groups for the studied compounds was benzo[c]thiophene (5) > thieno [3,2-b]thiophene (8) > 2,3-dihydrothieno[3,4-b][1,4]dioxine (7) > naphthalene (4) > butoxybenzene (1) > benzo[d]thiazole (3) > benzo[c][1,2,5]thiadiazole (2) > thieno[3,4-b]pyrazine (6). These results revealed that the DPP and AR fragments served as donors and CB fragments served as acceptors for 1, 4, 7, and 8. The DPP fragments served as donors and the AR and CB fragments served as acceptors for 2, 3, and 6. For 5, the DPP and CB fragments served as acceptors and AR fragment served as donors. Clearly, the vertical $S_0 \rightarrow S_1$ transitions for the current system possessed an intramolecular charge transfer (ICT) nature. The end groups affected the distributions of FMOs for the D- π -A- π -D molecules.

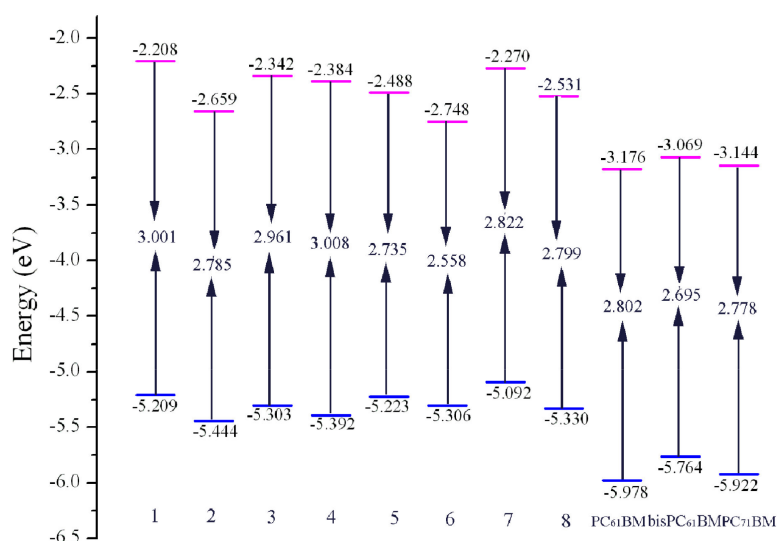


Figure 2. Evaluation of calculated FMO energies for investigated molecules as well as FMO energies for PC₆₁BM, bisPC₆₁BM, and PC₇₁BM at the PBE0/6-31G (d,p) level.

From the results displayed in Figure 2, it can be seen that the trends of E_{HOMO} and E_{LUMO} were $7 > 1 > 5 > 3 > 6 > 8 > 4 > 2$ and $1 > 7 > 3 > 4 > 5 > 8 > 2 > 6$, respectively. This suggests that molecules 2–6 and 8 were able to decrease the E_{HOMO} and E_{LUMO} compared with molecule 1. However, molecule 7 could increase/decrease the $E_{\text{HOMO}}/E_{\text{LUMO}}$ compared with that of molecule 1. Furthermore, the predicted E_g sequence was $4 > 1 > 3 > 7 > 8 > 2 > 5 > 6$. Obviously, molecules 2, 3, and 5–8 could narrow, whereas molecule 4 could decrease the E_g compared with that of molecule 1. Obviously, the introduction of benzo[c][1,2,5]thiadiazole (2), benzo[d]thiazole (3), benzo[c]thiophene (5), thieno[3,4-b]pyrazine (6), 2,3-dihydrothieno[3,4-b][1,4]dioxine (7), and thieno[3,2-b]thiophene (8) end groups led to narrower E_g values compared to molecules with a butoxybenzene (1) end group. However, the introduction of a naphthalene (4) end group decreased the E_g compared with that of molecule 1. This implied that the introduction of different AR fragments (donor groups) to the DPP led to the change of the E_{HOMO} , E_{LUMO} , and E_g values for its derivatives. These results indicated that these D- π -A molecules can lower the band gap and extend the absorption spectrum towards longer wavelengths. The absorption and fluorescence spectra can be tuned by donor groups. Consequently, the designed molecules except for 4 may possess longer absorption and fluorescence wavelengths

compared with those of molecule **1**. Therefore, it can be concluded that the E_{HOMO} , E_{LUMO} , and E_g of the designed D- π -A- π -D molecules can be tuned via different end groups.

2.2. Match between Donor and Acceptor Material

It is worth noting that the match between donor and acceptor is crucial for OSC devices. Namely, donor materials should possess suitable FMO energy levels. Firstly, with the aim of efficient electron transfer, the E_{LUMO} of the donor should be higher than that of the acceptor. Additionally, the $\Delta E_{\text{L-L}}$ should be larger than the binding energy (0.2–1.0 eV) [40,41], and should reach at least 0.3 eV. Secondly, in order to improve the performance of OSCs, donor materials should exhibit higher J_{sc} and V_{oc} values and efficient charge transfer. Therefore, lower E_{g} s are required for ensuring the successful harvesting of sunlight and to enhance the J_{sc} . A large difference between the E_{HOMO} of the donor and the E_{LUMO} of the acceptor is favorable for enhancing the V_{oc} and efficient exciton dissociation [42–45].

We took PC₆₁BM, bisPC₆₁BM, and PC₇₁BM as acceptors for the current system (see Figure 2). We calculated the $\Delta E_{\text{L-L}}$ of **1–8** (see Table 2). As visualized in Figure 2, the E_{LUMOS} of **1–8** were positioned above those of PC₆₁BM, bisPC₆₁BM, and PC₇₁BM, respectively. When PC₆₁BM, bisPC₆₁BM, and PC₇₁BM were taken as acceptors, the predicted $\Delta E_{\text{L-L}}$ of **1–8** was 0.428–0.968, 0.321–0.861, and 0.396–0.963 eV, respectively. Obviously, they are all exceeded 0.3 eV. As a consequence, the electron transfer to acceptors was efficient for these molecules. On the other hand, the E_{HOMO} of the designed molecules was lower by 1.916, 2.023, and 1.9481 eV than the E_{LUMO} of PC₆₁BM, bisPC₆₁BM, and PC₇₁BM, respectively. With the above considerations, the designed molecules possess suitable FMO energies to match those of the three typical fullerene acceptors. Therefore, the FMOs of these molecules can be tuned via planar electron-rich aromatic end groups to match PC₆₁BM, bisPC₆₁BM, and PC₇₁BM acceptors.

Table 2. The calculated $\Delta E_{\text{L-L}}$ values for **1–8** at the PBE0/6-31G (d,p).

Species	$\Delta E_{\text{L-L}}$ ^a	$\Delta E_{\text{L-L}}$ ^b	$\Delta E_{\text{L-L}}$ ^c
1	0.968	0.861	0.936
2	0.517	0.410	0.485
3	0.834	0.727	0.802
4	0.792	0.685	0.760
5	0.688	0.581	0.656
6	0.428	0.321	0.396
7	0.906	0.799	0.874
8	0.645	0.538	0.613

^a $\Delta E_{\text{L-L}}$ for PC₆₁BM as acceptor; ^b $\Delta E_{\text{L-L}}$ for bisPC₆₁BM as acceptor; ^c $\Delta E_{\text{L-L}}$ for PC₇₁BM as acceptor.

2.3. Absorption and Fluorescent Properties

Tables 3 and 4 collect the predicted properties of the absorption and fluorescence spectra of the designed molecules, respectively. The simulated absorption and fluorescence spectra of **1–8** are shown in Figures 3 and 4. For the absorption spectra, clearly, they were mainly derived from HOMO \rightarrow LUMO transitions with 71% contributions for **1–8**. The longest wavelengths of absorption (λ_{abs}) of molecules **2**, **3**, and **5–8** showed bathochromic shifts 43.4, 5.4, 52.1, 93.7, 29, and 36.1 nm, respectively, whereas molecule **4** exhibited a hypsochromic shift of 2.3 nm compared with molecule **1**. At the same time, the λ_{abs} was in the order of **6** > **5** > **2** > **8** > **7** > **3** > **1** > **4**, which was in excellent agreement with the corresponding reverse order of E_g values. Moreover, it was noted that molecules **6–8** had larger f value than that of **1**, while the while the corresponding f values of **2–5** were slightly less than that of **1**, respectively. Generally, a larger f value corresponds to a larger experimental absorption coefficient or stronger fluorescence intensity. This suggests that molecules **2**, **3**, and **5–8** were able to increase the λ_{abs} values compared with molecule **1**. On the other hand, molecule **4** did not significantly affect the λ_{abs} compared with molecule **1**. Therefore, the designed molecules can be used as donor materials for OSC applications.

Table 3. Predicted longest wavelengths of absorption, corresponding oscillator strength f , and main assignment of 1–8 at the TD-PBE0/6-31G (d,p)//PBE0/6-31G (d,p) level.

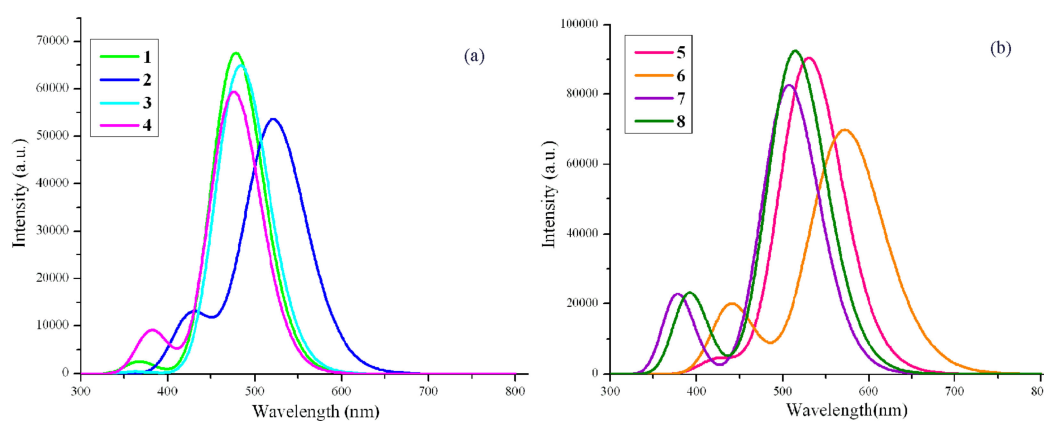
Species	λ_{abs} (nm)	f	Assignment
1	478.2	0.93	HOMO \rightarrow LUMO (0.71)
2	521.6	0.74	HOMO \rightarrow LUMO (0.70)
3	483.6	0.90	HOMO \rightarrow LUMO (0.71)
4	475.9	0.82	HOMO \rightarrow LUMO (0.71)
5	530.3	1.25	HOMO \rightarrow LUMO (0.71)
6	571.9	0.96	HOMO \rightarrow LUMO (0.70)
7	507.2	1.14	HOMO \rightarrow LUMO (0.71)
8	514.3	1.28	HOMO \rightarrow LUMO (0.70)
Exp ^a	494		

^a Experimental data for 1 were taken from Reference [39].

Table 4. Predicted longest wavelengths of fluorescence, corresponding oscillator strength f , and main assignment of 1–8 at the TD-PBE0/6-31G (d,p)//TD-PBE0/6-31G (d,p) level.

Species	λ_{flu}	f	Assignment
1	565.6	1.08	HOMO \leftarrow LUMO (0.71)
2	627.9	0.83	HOMO \leftarrow LUMO (0.71)
3	572.4	1.03	HOMO \leftarrow LUMO (0.71)
4	560.3	0.95	HOMO \leftarrow LUMO (0.71)
5	685.5	1.01	HOMO \leftarrow LUMO (0.71)
6	617.1	1.46	HOMO \leftarrow LUMO (0.71)
7	587.6	1.23	HOMO \leftarrow LUMO (0.71)
8	603.5	1.44	HOMO \leftarrow LUMO (0.71)
Exp ^a	562		

^a Experimental data for 1 were taken from Reference [39].

**Figure 3.** The calculated absorption spectra of the investigated molecules (value of full width at half maximum was 3000 cm^{-1}). (a) Molecules 1–4; (b) Molecules 5–8.

The longest wavelengths of fluorescence (λ_{flu}) of 1–8 mainly originated from the LUMO \rightarrow HOMO excitations, as shown in Table 4. Similar to those absorption spectra, the λ_{flu} of molecules 2, 3, and 5–8 showed bathochromic shifts 62.3, 6.8, 119.9, 51.5, 22, and 37.9 nm compared with molecule 1, respectively. In contrast, molecule 4 exhibited a hypsochromic shift of 5.3 nm compared with that of 1. The λ_{flu} values were in the sequence $5 > 2 > 6 > 8 > 7 > 3 > 1 > 4$. Furthermore, the f values of 2–5 were slightly less than that of 1 and the corresponding values of molecules 6–8 were larger than that of molecules 1, respectively. Therefore, the designed molecules had high fluorescent intensity. As a consequence, they can be used as luminescent materials for OLEDs, particularly for 6–8.

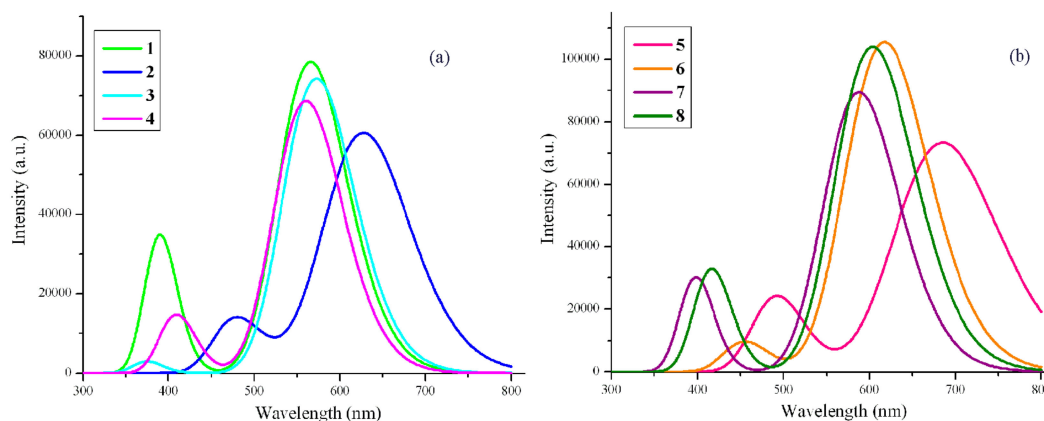


Figure 4. The calculated fluorescence spectra of the investigated molecules (value of full width at half maximum was 3000 cm^{-1}). (a) Molecules 1–4; (b) Molecules 5–8.

The results displayed in Tables 2 and 3 revealed that the absorption and fluorescence spectra of the designed molecules could be affected significantly by end groups. The designed molecules exhibited larger absorption coefficient and stronger fluorescence intensity. It suggests that these molecules could serve not only as luminescent for OLEDs, but also as donor materials in OSCs.

2.4. Reorganization Energies and Stabilities

The predicted λ_e and λ_h values of 1–8 are listed in Table 5. It was quite clear that the λ_h values of 1–8 were larger than those of λ_e , respectively. This suggested that rates of electron transfer may have been higher than rates of hole transfer for 1–8. Interestingly, molecule 1 possessed both the largest λ_e and λ_h values, indicating that the introduction of different end groups could lower the λ_e and λ_h for the designed molecules. Furthermore, molecules 5 and 6 exhibited the smallest λ_h and λ_e , respectively. From these results, it can be seen that the introduction of different end groups was favorable for hole and electron transfer. They may act as electron transport materials in OLEDs and OSCs.

Table 5. Calculated λ_e , λ_h , and η values (all in eV) of 1–8 at the PBE0/6-31G (d,p) level.

Species	λ_h	λ_e	η
1	0.401	0.343	2.284
2	0.374	0.240	2.174
3	0.386	0.322	2.277
4	0.364	0.315	2.305
5	0.325	0.260	2.104
6	0.356	0.222	2.017
7	0.392	0.278	2.180
8	0.380	0.263	2.145

Usually, the stability of materials can be predicted by means of the η value. As shown in Table 5, the η value of molecule 4 was larger than the value of molecule 1. However, as expected, molecules 2, 3, and 5–8 possessed slightly smaller than that of molecule 1. Compared with molecule 1, the stabilities of 2, 3 and 5–8 decreased slightly because of their steric hindrances. This suggested that the end groups had a little effect on the stability of molecules.

Another way to evaluate the stability of material is to analyze their electrostatic surface potentials. Therefore, the electrostatic surface potentials of the designed molecules were calculated and are plotted in Figure 5. The high negative charges of 1–8 resided at the two oxygen atoms of DPP moieties, as visualized in Figure 5. The reason for this may be the presence lone pairs on oxygen atoms. In contrast, partial positive charges were found on the aromatic end groups. It was observed that molecules 1–8 had similar positive and negative potential distributions, implying that they possessed

the same magnitude of photostability. Apparently, these results also revealed that the introduction of different end groups lightly affected on the stability of the molecules.

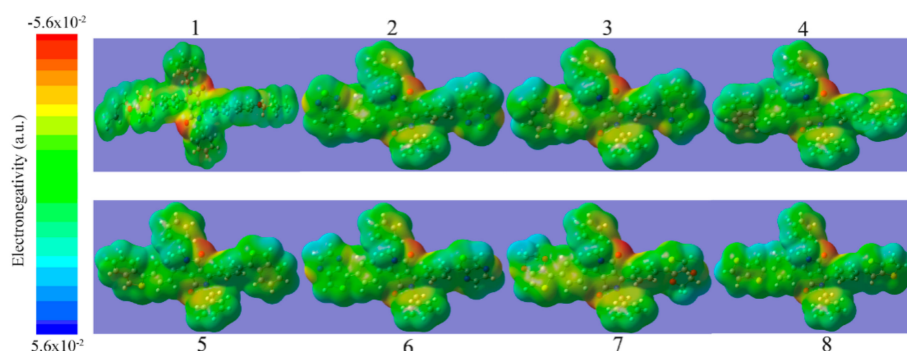


Figure 5. Electrostatic surface potentials for designed molecules. Regions of higher and lower electron density are shown in red and blue, respectively (values in atomic units).

3. Materials and Methods

Computational Methods

All the calculations were carried out using the Gaussian 09 suite of programs [46]. The DFT was employed to perform the geometry optimization and frequency calculations of the molecules in ground states (S_0). The frequency analysis characterized that the optimized structures are true minima. The equilibrium geometries of the molecules in the first excited singlet state (S_1) were optimized by mean of TD-DFT method. On the basis of the optimized structures in S_0 and S_1 , the absorption and fluorescent spectra were simulated by TD-DFT method, respectively. With the aim of choosing a choose reasonable method, different functionals were taken to optimize the geometry of **1** in S_0 and S_1 . These functionals contained, for example, B3LYP [47], PBE0 [48], CAM-B3LYP [49], M062X [50], MPW1PW91 [51], and ω B97XD [52]. Under the optimized structures in S_0 and S_1 , the absorption and fluorescent spectra of molecule **1** were predicted using the TD-DFT method. The λ_{abs} and λ_{flu} values are plotted in Figure 6. The tested results revealed that the λ_{abs} and λ_{flu} (478.2 and 565.6 nm) using the PBE0 (583 nm) method were well able to reproduce the experimental results (494 and 562 nm) [39], and the deviations were 15.8 and 3.6 nm, respectively. The Stokes shift was 87.4 nm, which was comparable to the experimental 68 nm. As a consequence, the PBE0 method was the best choice with which to investigate our system. The PBE0 method was also used to optimize the acceptors PC₆₁BM, bisPC₆₁BM, and PC₇₁BM. The 6-31G (d,p) basis set was used for all calculations.

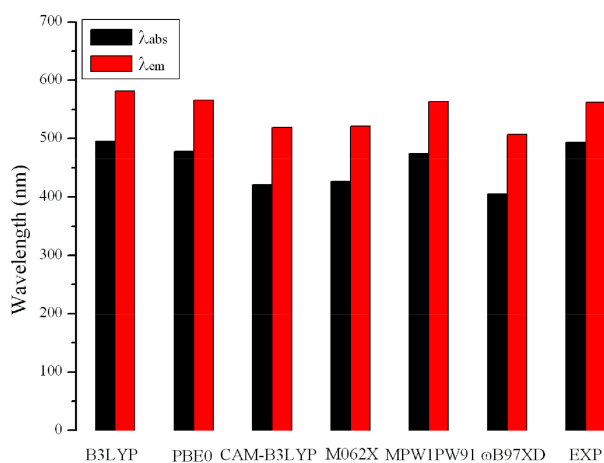


Figure 6. Calculated absorption and fluorescence wavelengths (λ_{abs} and λ_{flu}) of molecule **1** using various functionals, together with the experimental result.

It is commonly known that reorganization energy (λ) is a key parameter for charge transfer rates [53,54]. Lower electron (λ_e) and hole (λ_h) reorganization energies are beneficial for the higher electron and hole transfer rates, respectively. In this work, we only considered the internal λ , ignoring any environmental relaxation and changes. The λ_e and λ_h values were predicted at the PBE0/6-31G (d,p) level on the basis of the single-point energy. The λ_e and λ_h values were evaluated via the following equations [55]:

$$\lambda_e = (E_0^- - E_-^-) + (E_-^0 - E_0^0) \quad (1)$$

$$\lambda_h = (E_0^+ - E_+^+) + (E_+^0 - E_0^0) \quad (2)$$

where E_0^\pm is the energy of cation/anion structure based on the optimized neutral structure. Conversely, E_\pm^0 represents the energy of the neutral structure based on optimized cation/anion structure. Similarly, E_\pm^\pm is the energy of cation/anion structure based on the optimized cation/anion structure, while E_0^0 is the energy of the neutral molecule at ground state.

It was critically important to evaluate the stability of the material in OSC and OLED devices. The absolute hardness (η) of materials can be used as useful criterion with which to investigate the stability of the material. The η values can be predicted using the following equation [56,57]:

$$\eta = \frac{1}{2} \left(\frac{\partial \mu}{\partial N} \right) = \frac{1}{2} \left(\frac{\partial^2 E}{\partial N^2} \right) = \frac{AIP - AEA}{2} \quad (3)$$

where μ and N are the chemical potential and total electron number, respectively. *AIP* and *AEA* correspond to the adiabatic ionization potential and adiabatic electron affinity, respectively.

The *AIP* is the energy difference between the cation radical and its neutral species, while the *AEA* represents the energy difference between the neutral and its anion radical molecules. The PBE0/6-31G (d,p) method was applied to calculate the *AIP* and *AEA* values of the molecules. The electrostatic surface potentials can also be used to estimate the stability properties of molecules [58–60]. Therefore, we calculated the electrostatic surface potentials of molecules at the PBE0/6-31G (d,p) level.

4. Conclusions

Several D- π -A-type DPP-based small molecules were designed for OLED and OSC applications. Their photophysical and charge transfer properties were investigated using DFT and TD-DFT computational approaches. The calculated results revealed that the photophysical properties were affected through the introduction of different end groups. Furthermore, the electronic transitions corresponding to absorption and emission exhibited an intramolecular charge transfer feature. Additionally, the designed molecules possessed suitable FMO energies to match those of three typical fullerene acceptors, PC₆₁BM, bisPC₆₁BM, and PC₇₁BM. It was disclosed that the designed molecules acted not only as luminescent for OLEDs, but also as donor materials in OSCs. Moreover, they could also be used as potential electron transfer materials for OLEDs and OSCs.

Author Contributions: R.J. conceived and designed the calculations; X.Z. contributed to the performance and analysis of the frontier molecular orbitals and absorption and fluorescent spectra; W.X. performed the reorganization energies and transport properties; X.Z. helped with results interpretation. R.J. wrote the paper. All authors have read and agreed to the published version of the manuscript.

Funding: Financial supports from the NSFC (No. 21563002) are gratefully acknowledged.

Conflicts of Interest: The authors declare that they have no conflict of interest.

Abbreviations

OSCs	Organic solar cells
OLEDs	Organic light-emitting diodes
FETs	Field effect transistors
ΔE_{L-L}	Downhill energetic driving force

DPP	Diketopyrrolopyrrole
ICT	Intramolecular charge transfer
DFT	Density function theory
TD-DFT	Time dependent density function theory
FMOs	Frontier molecular orbital energies
HOMO	Highest occupied molecular orbital
LUMO	Lowest unoccupied molecular orbital

References

1. Zhao, J.; Li, Y.; Yang, G.; Jiang, K.; Lin, H.; Ade, H.; Ma, W.; Yan, H. Efficient organic solar cells processed from hydrocarbon solvents. *Nat. Energy* **2016**, *1*, 1–7. [[CrossRef](#)]
2. Fan, B.; Ying, L.; Zhu, P.; Pan, F.; Liu, F.; Chen, J.; Huang, F.; Cao, Y. All-polymer solar cells based on a conjugated polymer containing siloxane-functionalized side chains with efficiency over 10%. *Adv. Mater.* **2017**, *29*, 1703906. [[CrossRef](#)] [[PubMed](#)]
3. Meng, L.; Zhang, Y.; Wan, X.; Li, C.; Zhang, X.; Wang, Y.; Ke, X.; Xiao, Z.; Ding, L.; Xia, R.; et al. Organic and solution-processed tandem solar cells with 17.3% efficiency. *Science* **2018**, *361*, 1094–1098. [[CrossRef](#)] [[PubMed](#)]
4. Huo, Y.; Zhang, H.L.; Zhan, X. Non-fullerene all-small molecule organic solar cells. *ACS Energy Lett.* **2019**, *2*, 2717–2722.
5. Cui, Y.; Yao, H.; Hong, L.; Zhang, T.; Xu, Y.; Xian, K.; Gao, B.; Qin, J.; Zhang, J.; Wei, Z.; et al. Achieving over 15% efficiency in organic photovoltaic cells via copolymer design. *Adv. Mater.* **2019**, *31*, 1808356. [[CrossRef](#)] [[PubMed](#)]
6. Collins, S.D.; Ran, N.A.; Heiber, M.C.; Nguyen, T.Q. Small is powerful: Recent progress in solution-processed small molecule solar cells. *Adv. Energy Mater.* **2017**, *7*, 1602242. [[CrossRef](#)]
7. Han, L.; Wang, C.; Ren, A.; Liu, Y.; Liu, P. Structural and optical properties of triphenylamin-substituted anthracene derivatives. *J. Mol. Sci.* **2013**, *29*, 146–151.
8. Sahu, D.; Tsai, C.H.; Wei, H.Y.; Ho, K.C.; Chang, F.C.; Chu, C.W. Synthesis and applications of novel low bandgap star-burst molecules containing a triphenylamine core and dialkylated diketopyrrolopyrrole arms for organic photovoltaics. *J. Mater. Chem.* **2012**, *22*, 7945–7953. [[CrossRef](#)]
9. Coughlin, J.E.; Henson, Z.B.; Welch, G.C.; Bazan, G.C. Design and synthesis of molecular donors for solution-processed high-efficiency organic solar cells. *Acc. Chem. Res.* **2014**, *47*, 257–270. [[CrossRef](#)]
10. Huang, Y.; Zhang, M.; Chen, H.; Wu, F.; Cao, Z.; Zhang, L.; Tan, S. Efficient polymer solar cells based on terpolymers with a broad absorption range of 300–900 nm. *J. Mater. Chem. A* **2014**, *2*, 5218–5223. [[CrossRef](#)]
11. Koster, L.; Shaheen, S.; Hummelen, J. Pathways to a New Efficiency Regime for Organic Solar Cells. *Adv. Energy Mater.* **2012**, *2*, 1246–1253. [[CrossRef](#)]
12. Coffey, D.; Larson, B.; Hains, A.; Whitaker, J.; Kopidakis, N.; Boltalina, O.; Strauss, S.; Rumbles, G. An optimal driving force for converting excitons into free carriers in excitonic solar cells. *J. Phys. Chem. C* **2012**, *116*, 8916–8923. [[CrossRef](#)]
13. Song, X.; Gasparini, N.; Baran, D. The influence of solvent additive on polymer solar cells employing fullerene and non-fullerene acceptors. *Adv. Electron. Mater.* **2017**, *2*, 1700358. [[CrossRef](#)]
14. Song, X.; Gasparini, N.; Nahid, M.M.; Chen, H.; Macphree, S.M.; Zhang, W.; Norman, V.; Zhu, C.; Bryant, D.; Ade, H.; et al. A highly crystalline fused-ring n-type small molecule for non-fullerene acceptor based organic solar cells and field-effect transistors. *Adv. Funct. Mater.* **2018**, *28*, 1802895. [[CrossRef](#)]
15. Cheng, H.; Zhao, X.; Shen, Y.; Wang, M.; Wang, L.; Meier, H.; Cao, D. Diketopyrrolopyrrole based D- π -A- π -D type small organic molecules as hole transporting materials for perovskite solar cells. *J. Energy Chem.* **2018**, *27*, 1175–1182. [[CrossRef](#)]
16. Zhang, S.; Niu, Q.; Sun, T.; Li, Y.; Li, T.; Liu, H. The synthesis and properties of linear A- π -D- π -A type organic small molecule containing diketopyrrolopyrrole terminal units. *Spectrochim. Acta A* **2017**, *183*, 172–176. [[CrossRef](#)]
17. Zhang, S.; Sun, T.; Xu, Z.; Li, T.; Li, Y.; Niu, Q.; Liu, H. Novel biphenylene-diketopyrrolopyrrole-based A- π -D- π -A molecule: Synthesis, optical, electrochemical and electronical properties. *Tetrahedron. Lett.* **2017**, *58*, 2779–2783. [[CrossRef](#)]

18. Liu, H.; Jia, H.; Wang, L.; Wu, Y.; Zhan, C.; Fu, H.; Yao, J. Intermolecular electron transfer promoted by directional donor–acceptor attractions in self-assembled diketopyrrolopyrrole-thiophenefilms. *Phys. Chem. Chem. Phys.* **2012**, *14*, 14262–14269. [[CrossRef](#)]
19. Wang, M.; Wang, H.; Yokoyama, T.; Liu, X.; Huang, Y.; Zhang, Y.; Nguyen, T.Q.; Aramaki, S.; Bazan, G.C. High open circuit voltage in regioregular narrow band gap polymer solar cells. *J. Am. Chem. Soc.* **2014**, *136*, 12576–12579. [[CrossRef](#)]
20. Wang, E.; Mammo, W.; Andersson, M.R. 25th Anniversary article: Isoindigo-based polymers and small molecules for bulk heterojunction solar cells and field effect transistors. *Adv. Mater.* **2014**, *26*, 1801–1826. [[CrossRef](#)]
21. Chen, S.; Xiao, L.; Zhu, X.; Peng, X.; Wong, W.K.; Wong, W.Y. Solution-processed new porphyrin-based small molecules as electron donors for highly efficient organic photovoltaics. *Chem. Commun.* **2015**, *51*, 14439–14442. [[CrossRef](#)] [[PubMed](#)]
22. Walker, B.; Tamayo, A.B.; Dang, X.D.; Zalar, P.; Seo, J.H.; Garcia, A.; Tantiwivat, M.; Nguyen, T.Q. Nanoscale phase separation and high photovoltaic efficiency in solution-processed, small-molecule bulk heterojunction solar cells. *Adv. Funct. Mater.* **2009**, *19*, 3063–3069. [[CrossRef](#)]
23. Lin, Y.; Wang, Y.; Wang, J.; Hou, J.H.; Li, Y.F.; Zhu, D.B.; Zhan, X. A star-shaped perylene diimide electron acceptor for high-performance organic solar cells. *Adv. Mater.* **2014**, *26*, 5137–5142. [[CrossRef](#)]
24. Liu, Y.; Mu, C.; Jiang, K.; Zhao, J.; Li, Y.; Zhang, L.; Li, Z.; Lai, J.Y.L.; Hu, H.; Ma, T.; et al. A tetraphenylethylene corebased 3D structure small molecular acceptor enabling efficient non-fullerene organic solar cells. *Adv. Mater.* **2015**, *27*, 1015–1020. [[CrossRef](#)] [[PubMed](#)]
25. Mazzi, K.A.; Yuan, M.J.; Okamoto, K.; Luscombe, C.K. Oligoselenophene Derivatives Functionalized with a Diketopyrrolopyrrole Core for Molecular Bulk Heterojunction Solar Cells. *ACS Appl. Mater. Interfaces* **2011**, *3*, 271–278. [[CrossRef](#)] [[PubMed](#)]
26. Wu, Z.L.; Li, A.; Fan, B.; Xue, F.; Adachi, C.; Ouyang, J. Phenanthrene-functionalized 3,6-dithiophen-2-yl-2,5-dihydropyrrolo[3,4-c]pyrrole-1,4-diones as donor molecules for solution-processed organic photovoltaic cells. *Sol. Energy Mater. Sol. Cells.* **2011**, *95*, 2516–2523. [[CrossRef](#)]
27. Deng, J.; Chen, J.; Tao, Q.; Yan, D.; Fu, Y.; Tan, H. Improved photovoltaic performance of 2,7-pyrene based small molecules via the use of 3-carbazole as terminal unit. *Tetrahedron* **2018**, *74*, 3989–3995. [[CrossRef](#)]
28. Lin, Y.; Cheng, P.; Li, Y.; Zhan, X.A. A 3D star-shaped non-fullerene acceptor for solution-processed organic solar cells with a high open-circuit voltage of 1.18 V. *Chem. Commun.* **2012**, *48*, 4773–4775. [[CrossRef](#)]
29. Bürckstümmer, H.; Weissenstein, A.; Bialas, D.; Würthner, F. Synthesis and characterization of optical and redox properties of bithiophene-functionalized diketopyrrolopyrrole chromophores. *J. Org. Chem.* **2011**, *76*, 2426–2432. [[CrossRef](#)]
30. Huang, Y.F.; Chang, S.T.; Wu, K.Y.; Wu, S.L.; Ciou, G.T.; Chen, C.Y.; Liu, C.L.; Wang, C.L. Influences of conjugation length on organic field-effect transistor performances and thin film structures of diketopyrrolopyrrole-oligomers. *ACS Appl. Mater. Interfaces* **2018**, *10*, 8869–8876. [[CrossRef](#)]
31. Ha, J.S.; Kim, K.H.; Choi, D.H. 2,5-Bis(2-octyldodecyl)pyrrolo[3,4-c]pyrrole-1,4-(2H,5H)-dione-based donor-acceptor alternating copolymer bearing 5,5'-di(thiophen-2-yl)-2,2'-biselenophene exhibiting $1.5 \text{ cm}^2 \cdot \text{v}^{-1} \cdot \text{s}^{-1}$ hole mobility in thin-film transistors. *J. Am. Chem. Soc.* **2011**, *133*, 10364–10367. [[CrossRef](#)] [[PubMed](#)]
32. Tang, M.; Wu, S.; Xing, W.; Shen, H.; Xiang, L.; Liang, Y.; Xu, W.; Zhu, D. Diketopyrrolopyrrole based small molecular semiconductors containing thiazole units for solution-processed n-channel thin-film transistors. *Dye Pigment.* **2019**, *163*, 707–714. [[CrossRef](#)]
33. Ponsot, F.; Bucher, L.; Desbois, N.; Rousselin, Y.; Mondal, P.; Devillers, C.H.; Romieu, A.; Gros, C.P.; Singhal, R.; Sharma, G.D. A bacteriochlorin-diketopyrrolopyrrole triad as a donor for solution-processed bulk heterojunction organic solar cells. *J. Mater. Chem. C* **2019**, *7*, 9655–9664. [[CrossRef](#)]
34. Song, X.; Gasparini, N.; Nahid, M.M.; Paleti, S.H.K.; Li, C.; Li, W.; Ade, H.; Baran, D. Efficient DPP donor and nonfullerene acceptor organic solar cells with high photon-to-current ratio and low energetic loss. *Adv. Funct. Mater.* **2019**, *29*, 1902441. [[CrossRef](#)]
35. He, X.; Yin, L.; Li, Y. Efficient design and structural modifications for tuning the photoelectric properties of small molecule acceptors in organic solar cells. *New J. Chem.* **2019**, *43*, 6577–6586. [[CrossRef](#)]
36. Zhao, C.; Guo, Y.; Zhang, Y.; Yan, N.; You, S.; Li, W. Diketopyrrolopyrrole-based conjugated materials for non-fullerene organic solar cells. *J. Mater. Chem. A* **2019**, *7*, 10174–10199. [[CrossRef](#)]

37. Roland, T.; Heyer, E.; Liu, L.; Ruff, E.; Ludwigs, S.; Ziessel, R.; Haacke, S. Unsymmetrical donor-acceptor-acceptor- π -donor type benzothiadiazole-based small molecule for a solution processed bulk heterojunction organic solar cell. *ACS Appl. Mater. Interfaces* **2015**, *7*, 10283–10292.
38. Heyer, E.; Ziessel, R. Panchromatic push-pull dyes of elongated form from triphenylamine, diketopyrrolopyrrole, and tetracyanobutadiene modules. *Synlett* **2015**, *26*, 2109–2116.
39. Kuwabara, J.; Yamagata, T.; Kanbara, T. Solid-state structure and optical properties of highly fluorescent diketopyrrolopyrrole derivatives synthesized by cross-coupling reaction. *Tetrahedron* **2010**, *66*, 3736–3741. [[CrossRef](#)]
40. Knupfer, M. Exciton binding energies in organic semiconductors. *Appl. Phys. A* **2003**, *77*, 623–626. [[CrossRef](#)]
41. Hill, I.G.; Kahn, A.; Soos, Z.G.; Pascal, R.A., Jr. Charge-separation energy in films of π -conjugated organic molecules. *Chem. Phys. Lett.* **2000**, *327*, 181–188. [[CrossRef](#)]
42. Li, J.; Ong, K.H.; Lim, S.L.; Ng, G.M.; Tan, H.S.; Chen, Z.K. A random copolymer based on dithienothiophene and diketopyrrolopyrrole units for high performance organic solar cells. *Chem. Commun.* **2011**, *47*, 9480–9482. [[CrossRef](#)] [[PubMed](#)]
43. Choi, Y.S.; Jo, W.H. A strategy to enhance both Voc and Jsc of A-D-A type small molecules based on diketopyrrolopyrrole for high efficient organic solar cells. *Org. Electron.* **2013**, *14*, 1621–1628. [[CrossRef](#)]
44. Stuart, A.C.; Tumbleston, J.R.; Zhou, H.; Li, W.; Liu, S.; Ade, H.; You, W. Fluorine substituents reduce charge recombination and drive structure and morphology development in polymer solar cells. *J. Am. Chem. Soc.* **2013**, *135*, 1806–1815. [[CrossRef](#)]
45. Kim, H.; Lee, H.; Seo, D.; Jeong, Y.; Cho, K.; Lee, J.; Lee, Y. Regioregular low bandgap polymer with controlled thieno[3,4-b]thiophene orientation for high efficiency polymer solar cells. *Chem. Mater.* **2015**, *27*, 3102–3107. [[CrossRef](#)]
46. Frisch, M.J.; Trucks, G.W.; Schlegel, H.B.; Scuseria, G.E.; Robb, M.A.; Cheeseman, J.R.; Scalmani, G.; Barone, V.; Mennucci, B.; Petersson, G.A.; et al. *Gaussian 09*; Gaussian, Inc.: Wallingford, CT, USA, 2009.
47. Becke, A.D. Density functional thermochemistry. III. The role of exact exchange. *J. Chem. Phys.* **1993**, *98*, 5648–5652. [[CrossRef](#)]
48. Adamo, C.; Barone, V. Toward reliable density functional methods without adjustable parameters: The PBE0 model. *J. Chem. Phys.* **1999**, *110*, 6158–6170. [[CrossRef](#)]
49. Yanai, T.; Tew, D.P.; Handy, N.C. A new hybrid exchange–correlation functional using the coulomb-attenuating method (CAM-B3LYP). *Chem. Phys. Lett.* **2004**, *393*, 51–57. [[CrossRef](#)]
50. Zhao, Y.; Truhlar, D.G. The M06 suite of density functionals for main group thermochemistry, thermochemical kinetics, noncovalent interactions, excited states, and transition elements: Two new functionals and systematic testing of four M06-class functionals and 12 other functionals. *Theor. Chem. Acc.* **2008**, *120*, 215–241.
51. Adamo, C.; Barone, V. Exchange functionals with improved long-range behavior and adiabatic connection methods without adjustable parameters: The mPW and mPW1PW models. *J. Chem. Phys.* **1998**, *108*, 664–675. [[CrossRef](#)]
52. Chai, J.D.; Head-Gordon, M.H.H. Toward reliable density functional methods without adjustable parameters: The PBE0 model. *Phys. Chem. Chem. Phys.* **2008**, *10*, 6615–6620. [[CrossRef](#)]
53. Marcus, R.A. Chemical and electrochemical electron-transfer theory. *Annu. Rev. Phys. Chem.* **1964**, *15*, 155–196. [[CrossRef](#)]
54. Marcus, R.A. Electron transfer reactions in chemistry. Theory and experiment. *Rev. Mod. Phys.* **1993**, *65*, 599–610. [[CrossRef](#)]
55. Köse, M.E.; Mitchell, W.J.; Kopidakis, N.; Chang, C.H.; Shaheen, S.E.; Kim, K.; Rumbles, G. Theoretical studies on conjugated phenyl-cored thiophene dendrimers for photovoltaic applications. *J. Am. Chem. Soc.* **2007**, *129*, 14257–14270. [[CrossRef](#)]
56. Pearson, R.G. Absolute electronegativity and absolute hardness of Lewis acids and bases. *J. Am. Chem. Soc.* **1985**, *107*, 6801–6806. [[CrossRef](#)]
57. Start, M.S. Epoxidation of alkenes by peroxy radicals in the gas phase: Structure–activity relationships. *J. Phys. Chem. A* **1997**, *101*, 8296–8301. [[CrossRef](#)]
58. Chaudhry, A.R.; Ahmed, R.; Irfan, A.; Muhammad, S.; Shaari, A.; Al-Sehemi, A.G. Influence of push–pull configuration on the electro-optical and charge transport properties of novel naphtho-difuran derivatives: A DFT study. *RSC Adv.* **2014**, *4*, 48876–48887. [[CrossRef](#)]

59. Irfan, A.; Zhang, J. Effect of one ligand substitution on charge transfer and optical properties in mer-Alq₃: A theoretical study. *Theor. Chem. Acc.* **2009**, *124*, 339–344. [[CrossRef](#)]
60. Chaudhry, A.R.; Ahmed, R.; Irfan, A.; Shaari, A.; Al-Sehemi, A.G. Effects of electron withdrawing groups on transfer integrals, mobility, electronic and photo-physical properties of naphtho[2,1-b:6,5-b]difuran derivatives: A theoretical study. *Sci. Adv. Mater.* **2014**, *6*, 1727–1739. [[CrossRef](#)]

Sample Availability: Not available.



© 2020 by the authors. Licensee MDPI, Basel, Switzerland. This article is an open access article distributed under the terms and conditions of the Creative Commons Attribution (CC BY) license (<http://creativecommons.org/licenses/by/4.0/>).